Loschmidt echo, emerging dual unitarity and scaling of generalized temporal entropies after quenches to the critical point

Stefano Carignano
Barcelona Supercomputing Center, 08034 Barcelona, Spain*

Luca Tagliacozzo

Institute of Fundamental Physics IFF-CSIC, Calle Serrano 113b, Madrid 28006, Spain[†]

The Loschmidt echo of a product state after a quench to a conformal invariant critical point can be predicted by using conformal field theories (CFT). We check such prediction with tensor networks, finding excellent agreement. In particular, we are able to predict and confirm that the CFT imply an emerging dual-unitarity of the evolution. We show how to extract the universal information of the underlying CFT including, the central charge, the operator content, and the generalized temporal entropies. Our results also imply that, using state-of-the art tensor networks algorithms, such calculations only require resources that increase polynomially with the duration of the quench, thus providing an example of numerically efficiently solvable out-of-equilibrium scenario.

Introduction. Strongly-correlated quantum systems still defy our understanding under many aspects. The situation is especially complicated out-of-equilibrium, where even the existence of non-ergodic phases such as the many-body localized phase is still highly debated [1, 2]. As a result, most of our understanding of the outof-equilibrium dynamics emerges from either integrable models [3–6], conformal field theories [7–12], Floquet systems such as random circuits [13] or dual unitary models [14–18]. The latter are particularly interesting since they provide an analytic framework for computing interesting quantities without being integrable, thus providing access to both ergodic and non-ergodic dynamics. Recently, dual unitary gates have been used to construct tov models for holography which display emerging discrete Lorentz and conformal invariance [19].

Here, we provide an example in the other direction, showing that quenches described by conformal field theories (CFT) provide examples of emerging dual-unitary dynamics in an Hamiltonian setting. The underlying Lorentz invariance induces a linear dispersion relation of the low-energy excitations and thus, in the field theory, the propagation of the information with a single velocity. This feature is shared by the dual unitary dynamics, where there is a single speed for the propagation of the correlations.

In order to unveil the emergence of a dual unitary dynamics in the thermodynamic limit, we characterise the return probability of an initial product state after a quench to the critical conformal invariant point. In particular, we show how to define a transverse transfer matrix (TM) whose spectrum becomes, in the continuum and for large times, that of a unitary matrix. Such spectrum is fixed by the operator content of the CFT [20, 21]. We also show that the return probabilities contain the usual Casimir-like terms proportional to the central charge [22, 23]. Finally, we show that the generalized temporal entropy of the leading eigenvectors of such

TM are well described by the predictions obtained from holography and CFT initially derived in [24–30], that can be easily re-derived in our framework. In order to check such predictions, we provide tensor networks (TN) simulations based on our recently introduced algorithm [36] of two exemplary minimal models, the Ising and the three-states Potts model, finding perfect agreement with the CFT predictions.

Our calculations also show how transverse TN contractions can be used to give access to the Loschmidt echo in strongly correlated one-dimensional systems directly in the thermodynamic limit, with a cost that only increases polynomially with the duration of the quench. Such echo can be used as a probe of quantum chaos and its behavior can be related to that of out-of-time ordered correlations [37] (for a review see [38]). The possibility to evaluate these quantities for arbitrarily long times is thus of paramount importance.

Setup and CFT predictions. Given a 1D quantum many-body system made by L constituents and described by a Hamiltonian H, we focus on the contraction of a TN encoding the Loschmidt echo, namely the return probability of a state of a system to its initial state after the out-of-equilibrium evolution for a time T, and its intensive part,

$$\mathcal{L} = |\langle \psi_0 | e^{-iHT} | \psi_0 \rangle|, \quad l = -\frac{\log \mathcal{L}}{TL}.$$
 (1)

Such an intensive part is finite and plays the role of the free-energy in statistical mechanics.

Our setup is described in Fig. 1(a-c): through simple tensor decompositions, we can express the evolution for an infinitesimal time step $U(\delta t)$ as a matrix product operator (MPO) with finite bond dimension (see e.g. [39, 40]). As a result, the full (1) is given by the contraction of a

¹ For similar algorithms see also [31–35].

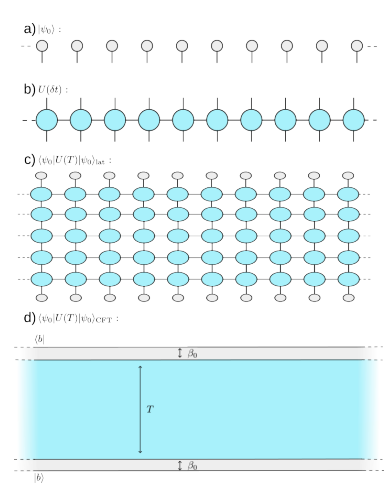


FIG. 1. The Loschmidt echo can be studied numerically by defining the tensor network made by a) the initial product state b) the MPO of the evolution operator and c) its matrix element. It can also be characterized using field theories, by analytically continuing the results obtained by mapping the CFT on the plane to the finite geometries shown in d). The field theory infrared divergence is handled by studying a finite spatial extent L that is then sent to infinity, while the UV divergencies are cured by introducing a finite β_0 close to the conformally invariant boundary states $|b\rangle$.

regular 2D TN made by $L \times N_T$ ($N_T = T/\delta t$) elementary four-leg tensors, one for every space-time point. Since everything is translationally invariant, we can directly consider the thermodynamic limit by sending $L \to \infty$, thus building an infinite strip with a width of N_T tensors in the time direction.

We focus on critical dynamics and thus use the machinery of CFTs. In the CFT, the initial states are conformally invariant boundary states $|b\rangle$ [9, 21] and the Loschmidt echo is described by the geometry illustrated in Fig. 1(d), representing an infinite long strip with transverse size $T+2\beta_0$ and with boundary conditions given by the chosen $|b\rangle$. On the lattice, we accordingly evolve an initial product state corresponding to $|b\rangle$ for some short amount of euclidean time β_0 [7–9, 41]. The Loschmidt echo for a product state is obtained by taking the limit $\beta_0 \to 0$.

Following well-established prescriptions [7, 8, 41], we obtain predictions for the real-time calculations by performing an analytic continuation of the results of CFTs in Euclidean space. We start with the standard results on an infinite strip² with imaginary extent β and analytically continue them to the case $\beta = iT + 2\beta_0$ [7, 27, 28, 42]. The CFT predictions at finite β are ob-

The transfer operator \mathcal{T} produces translations along s. It is given by $\mathcal{T} = exp(\int du \mathbb{T}_{ss} \Delta s)$, where \mathbb{T} represents the stress-energy tensor of the CFT and Δs is the UV cutoff in the spatial direction. Since all these constructions are well described in the CFT literature, here we only cite the relevant results. In particular, the TMs describing our quench are given by

$$\mathcal{T} = \exp\left[-\frac{\kappa_s}{\beta v} + \frac{\pi}{\beta v}L_0 + \mathcal{O}\left(\frac{1}{(\beta v)^2}\right)\right],\tag{2}$$

where $\kappa_s = -\pi c \delta t/24$, L_0 is the relevant generator of the Virasoro algebra and c is the central charge [43–48]. In the following, we will neglect for brevity the higher-order terms $\mathcal{O}(1/\beta^2)$ from the CFT expansion (2), which will not play a role for larger T.

If we now define $\{\tau_i\}$ the eigenvalues of \mathcal{T} (with $|\tau_0| > |\tau_1| > \dots$) and $\lambda_i = \log(-\tau_i)$, one can see that the intensive part l of the Loschmidt echo is dictated by λ_0 , the logarithm of the leading eigenvalue of \mathcal{T} , as l converges to $-\frac{|\lambda_0|}{T}$ exponentially in the thermodynamic limit for a gapped \mathcal{T} . The important relation in Eq. (2) identifies the full spectrum of \mathcal{T} with that of L_0 , which is diagonal in the basis of scaling fields. As a result, the CFT predicts the full spectrum of \mathcal{T} , which is given by the operator content of the corresponding CFT with boundaries [20, 21].

As usual when working on the lattice we have to add to the CFT predictions the non-universal terms caused by e.g. the normalization of the Hamiltonian and the boundary effects [22, 23]. In particular, the logarithm of the leading eigenvalue of \mathcal{T} scales as

$$\lambda_0^{CFT} = a\beta v + b + \frac{\kappa}{\beta v}, \qquad (3)$$

where a plays the role of the non-universal ground state energy and b of the boundary contributions.

After analytically continuing Eq. (3), we find

$$Re(\lambda_0) = 2\beta_0 av + b\,, (4)$$

$$Im(\lambda_0) = avT - \frac{\kappa}{vT}, \qquad (5)$$

while for the first gap the analytical continuation of the CFT results gives (up to higher-order corrections) $Re(\lambda_1 - \lambda_0) = 0$ and

$$Im(\lambda_1 - \lambda_0) = -\frac{p\pi x_1}{vT}, \qquad (6)$$

tained by using conformal maps³: The infinite strip described by complex coordinate w=s+iu, related to the upper 2D plane by the map $w'=\frac{v\beta}{\pi}\log(z)$, where v is the sound velocity.

² For completeness, we recall analogous results for a cylinder in the Supplementary Material.

³ Explicit CFT predictions for the Loschmidt echo after local quenches have been obtained in [9].

where x_1 is the smallest boundary critical exponent. The CFT predictions extend to the whole spectrum of \mathcal{T} , dictating that all its gaps shrink to zero as T increases, and are determined by the various Kac modules of the theory encoding the primaries and their descendents, which are selected by the boundary conditions [21, 49].

These results thus unveil a connection between the CFTs and dual unitary evolutions: up to higher-order corrections, which vanish as T increases, \mathcal{T} has full sectors of gaps that are purely imaginary, and collapse on the unit circle for $\beta_0 \to 0$. This suggests that \mathcal{T} becomes unitary in the limit of $T \to \infty$.

We can extract even more informations from the CFT. In particular, the scaling of the two point function

$$\langle \phi(\omega_1)\phi(\omega_2)\rangle = \left(\frac{\pi}{\beta v}\right)^{2x} \sin\left[\frac{\pi}{\beta v}\left(u_1 - u_2\right)\right]^{-2x}, \quad (7)$$

for twist fields where x becomes $\Delta_n = \frac{c}{24} (n - 1/n)$, gives access to the Tsallis entropies of order n [50–54].

In Eq. (7) we are considering purely imaginary distances $u_1 - u_2$ on the CFT complex strip, so that we can use it to predict the behavior of the traces of the *n*-th power of the reduced transition matrices, defined as⁴

$$\mathcal{T}_{t}^{L|R} = \operatorname{tr}_{N_{t}-t} \left[\mathcal{T}^{L|R} \right], \quad \mathcal{T}^{L|R} = \frac{|R\rangle \langle L|}{\langle L|R\rangle}, \quad (8)$$

where $|R\rangle$ and $\langle L|$ are the right and left dominant eigenvectors of \mathcal{T} . By continuing Eq. (7) to n=1 we obtain the results for the generalized entanglement entropies [26] of $|R\rangle$ and $\langle L|$, which the limit of small β_0 , by replacing $\beta \to iT$, $u_1 - u_2 \to it$, becomes

$$S_{gen} = s_0 + \frac{i\pi c}{12} + \frac{c}{6} \log \left[\frac{2T}{\pi} \sin \left(\frac{\pi t}{T} \right) \right], \qquad (9)$$

with s_0 a constant.

Notice that even though \mathcal{T} becomes unitary, the leading eigenvectors only have logarithmic generalized entropies. This fact is due to the CFT Hilbert space structure, whose number of states (at low energy) only diverges polynomially with T. The small finite β_0 project onto that subspace. Similar effects have been observed in [41, 55, 56].

We can now check the above results using matrix product states (MPS). As in standard TN approaches, we define a transfer-matrix temporal MPO (tMPO) \mathcal{T} by contracting a vertical strip of tensors, and find its leading left and right eigenvectors in the form of temporal MPS (tMPS) [31–35, 57] as shown in Fig. 2 (see Supplementary Material for more details on the algorithm).

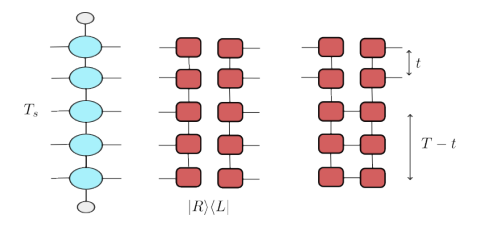


FIG. 2. The transverse transfer matrix \mathcal{T} involves the contraction of a column of elementary tensors a). Its leading left and right eigenvectors b) allow to characterize the Loschmidt echo (1) in the thermodynamic limit. Generalized temporal entropies are extracted from the reduced transition matrices defined in Eq. (8).

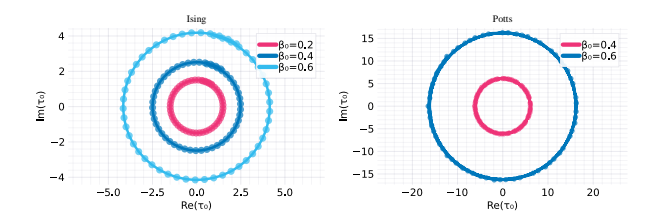


FIG. 3. Real vs imaginary parts of τ_0 , the dominant eigenvalue of \mathcal{T} for various values of T and β_0 for the Ising (left) and Potts (right) models. For a fixed β_0 , as we vary T they distribute on an almost constant radius circle.

Numerical results. We consider both the transverse field Ising model with Hamiltonian

$$H_{Ising}(g) = -\sum_{i} \left[\sigma_x^i \sigma_x^{i+1} + g \sigma_z^i \right], \tag{10}$$

where σ_x, σ_z are the Pauli matrices, and the three-state Potts model

$$H_{Potts}(g) = -\sum_{i} \left[\left(\sigma_{i} \sigma_{i+1}^{\dagger} + \sigma_{i}^{\dagger} \sigma_{i+1} \right) + g(\tau_{i} + \tau_{i}^{\dagger}) \right], (11)$$

with the matrices $\sigma = \sum_{s=0,1,2} \omega^s |s\rangle \langle s|, \omega = e^{i2\pi/3}$ and $\tau = \sum_{s=0,1,2} |s\rangle \langle s+1|$, where the addition is modulo 3. In both cases, the critical point (g=1) is described by a CFT. We consider different tMPO's lengths T, which acts as IR cutoff, investigating also the dependence of the results on β_0 having the role of a UV cutoff. In order to make more connections with the CFT, we will consider both free and fixed boundary conditions (BC). In our formulation, the former corresponds to a $|\uparrow\rangle$ state for Ising and a $|111\rangle / \sqrt{3}$ state for Potts, while the latter is a $|+\rangle$ state in Ising and $|001\rangle$ in Potts [58]. Our calculations are performed using a Trotter step of $\delta t=0.1$.

Transfer matrix spectra. As we vary the length T of the tMPO \mathcal{T} with β_0 fixed, its dominant eigenvalues become distributed over circles (see Fig. 3), whose radius quickly collapses to a constant as T increases, consistent with the predictions of Eq. (5). We obtain the value of κ in the same equation from which we extract c by fitting the

⁴ Notice that the sine in Eq. (7) is the result of the choice of the cut in the path integral that lies in the time direction.

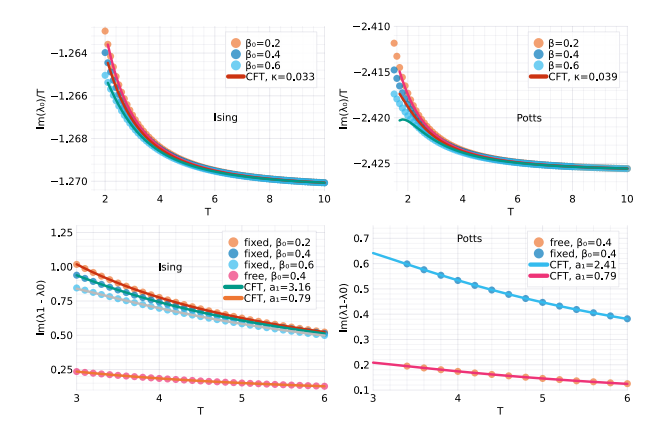


FIG. 4. Top row: Imaginary parts of λ_0 for different values of β_0 . The points are data from our TN calculation, solid lines are fits using the expected CFT form, which we use to extract the value of the central charge (see main text). The fits show an excellent agreement with data for larger T, as expected. Bottom row: Imaginary part of the first gap $\lambda_1 - \lambda_0$ for different β_0 and BC, and corresponding fits to the CFT formulas to extract x_1 . Left: Results for the Ising model, Right: Potts model.

numerical results for $Im(\lambda_0)/T$ with a functional form $f_1(T) = a_0 + \kappa/T^2 + a_4/T^4$.

The results for different values of β_0 are shown in Fig. 4 (top). All of them give comparable results, for Ising we obtain $a_0 \simeq 1.27$ and $\kappa \simeq 0.032$, which from Eq. (5) with $v = v_{Ising} = 2$ [57], gives $c_{fit} = 0.49$, in excellent agreement with $c_{Ising} = 1/2$. For Potts, the fits give $\kappa \simeq 0.039$ and using for the velocity $v_{Potts} \simeq 3\sqrt{3}/2$ [59] we obtain a value $c_{fit} \simeq 0.78$, compatible with the expected $c_{Potts} = 4/5$. A similar analysis for the real part of λ_0 in the Supplementary Materials also confirms the CFT predictions.

From the first excitation λ_1 of \mathcal{T} we extract the first gap. Focusing again on the imaginary parts, we fit $Im(\lambda_1 - \lambda_0)$ with $f_3(T) = a_1/T + a_3/T^3$, inspired by Eq. (6), see Fig. 4 (bottom). The results also confirm the CFT predictions [21]: For the Ising model with fixed BC we obtain $a_1 \simeq 3.155$, in agreement with $\pi x_1/v_{Ising}$ for $x_1 = 2$. For free BC we get instead $a_1 = 0.786 \simeq \pi/4$, consistent with $x_1 = 1/2$. For Potts, we obtain $a_1 \simeq 0.788$ for free BC and $a_1 \simeq 2.41$ for fixed BC state, respectively. This corresponds to $x_1 = v_{Potts}a_1/\pi \simeq 0.65$ and 1.98, which we can match with the expected 2/3 for the free and 2 for fixed boundary conditions [21, 49].

Generalized entropies. The (complex-valued) generalized entropies are obtained from the dominant eigenvectors of the TM. They have an holographic meaning [24–30, 60], and provide a measure for the complexity of the TN contraction and thus for the cost for simulating the Loschmidt echo with tensor networks [31, 33, 35, 36]. The results in Fig. 5 show that both for Ising and Potts the agreement with the CFT predictions is excellent already

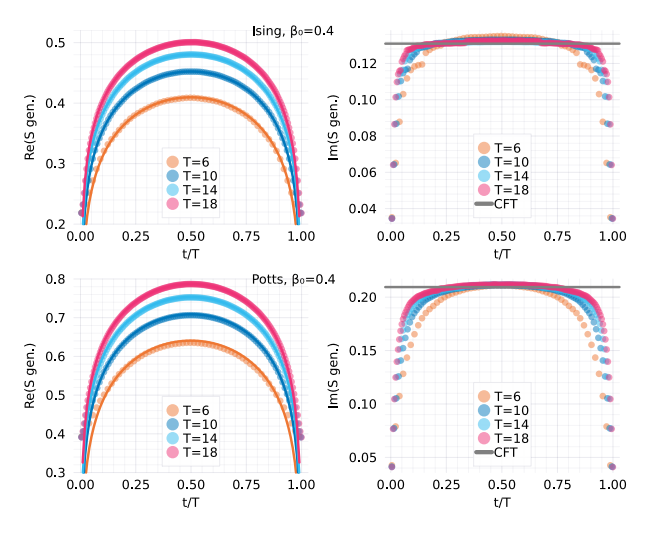


FIG. 5. Numerical results for the real (left) and imaginary (right) parts of the generalized entropies for the critical Ising (top row) and critical Potts (bottom row) with free BC. Solid lines denote the CFT predictions (9). For Ising, we use c=1/2 central charge and $s_0=0.3$ the constant providing the best match for the real part, whereas for Potts we use the central charge c=4/5 and $s_0=0.46$. The agreement with the CFT predictions is excellent for both real and imaginary parts, and it improves as we go to longer chains, as expected.

for relatively short T. Neglecting the boundary effects, the imaginary part of the entropy becomes constant and matches the expected $Im(S_{\rm CFT}) = \pi c/12$, and the real part is well fitted by Eq. (9) 5 . Our numerical results also validate equivalent predictions for the generalized entropies which have been obtained with different techniques based on holography and CFTs in [26, 28, 42, 61].

Conclusions We have shown that the time evolution operator generated by a critical Hamiltonian gives rise to a unitary transfer matrix in space, something that one would expect for dual unitary evolutions. Conformal symmetry thus seems to imply an emerging dual unitary dynamics. This is just one of the results we obtain by extracting the CFT predictions for the Loschmidt echo after a global quench. All these predictions are confirmed by state-of-the art numerical simulations using TNs. We observe a special class of transverse unitary evolution, whose leading eigenvectors's entropy only increase logarithmically with time rather than linearly as one would expect. We believe this is a consequence of the ultraviolet regularization induced by β_0 . In other contexts similar regularizations have been used [41, 55, 56] so our work provides some analytical insight on those results

⁵ Different boundary conditions can affect the rate of convergence of the curves to the CFT predictions. We discuss this fact in detail in the Supplementary Material.

too. Our results also open the way to applying tensor networks for studying the Loschmidt echo for long times, allowing to provide definite answers to open problems along the lines of the recent approaches [62–67].

We would like to thank M.C. Bañuls, P. Calabrese, E. Lopez, G. Sierra, E. Tonni for discussions related to this project. We thank A. Tomut for suggesting the reference [58] clarifying the role of the lattice BC for the Potts model. LT acknowledges support from the Proyecto Sinérgico CAM Y2020/TCS-6545 NanoQuCo-CM, the CSIC Research Platform on Quantum Technologies PTI-001, and from the Grant TED2021-130552B-C22 funded by MCIN/AEI/10.13039/501100011033 and by the "European Union NextGenerationEU/PRTR", and Grant PID2021-127968NB-I00 funded by MCIN/AEI/10.13039/501100011033.

- * stefano.carignano@bsc.es † luca.tagliacozzo@iff.csic.es
- [1] JCCMP, Whither many-body localization? (2023).
- [2] A. Chandran and P. Crowley, Physics 17, 24 (2024).
- [3] J.-S. Caux and F. H. L. Essler, Phys. Rev. Lett. 110, 257203 (2013).
- [4] F. H. L. Essler and A. J. J. M. de Klerk, Statistics of matrix elements of local operators in integrable models (2023), arxiv:2307.12410 [cond-mat].
- [5] B. Bertini, M. Collura, J. De Nardis, and M. Fagotti, Phys. Rev. Lett. 117, 207201 (2016).
- [6] O. A. Castro-Alvaredo, B. Doyon, and T. Yoshimura, Phys. Rev. X 6, 041065 (2016).
- [7] P. Calabrese and J. Cardy, J. Stat. Mech. 2005, P04010 (2005).
- [8] P. Calabrese and J. Cardy, J. Stat. Mech. 2007, P10004 (2007).
- [9] J.-M. Stéphan and J. Dubail, J. Stat. Mech. 2011, P08019 (2011).
- [10] J. Cardy and E. Tonni, J. Stat. Mech.: Theory Exp. 2016 (12), 123103.
- [11] J. Dubail, J. Phys. A: Math. Theor. 50, 234001 (2017), arxiv:1612.08630 [cond-mat, physics:hep-th, physics:quant-ph].
- [12] J. Surace, L. Tagliacozzo, and E. Tonni, Phys. Rev. B 101, 241107 (2020).
- [13] A. Nahum, J. Ruhman, S. Vijay, and J. Haah, Phys. Rev. X 7, 031016 (2017), arxiv:1608.06950 [cond-mat, physics:hep-th, physics:quant-ph].
- [14] B. Bertini, P. Kos, and T. Prosen, Phys. Rev. Lett. 121, 264101 (2018), arxiv:1805.00931 [cond-mat, physics:hepth, physics:nlin, physics:quant-ph].
- [15] B. Bertini, P. Kos, and T. Prosen, Phys. Rev. X 9, 021033 (2019).
- [16] B. Bertini, P. Kos, and T. Prosen, Phys. Rev. Lett. 123, 210601 (2019).
- [17] P. W. Claeys and A. Lamacraft, Phys. Rev. Research 2, 033032 (2020), arxiv:2003.01133 [cond-mat, physics:nlin, physics:quant-ph].
- [18] P. W. Claeys and A. Lamacraft, Phys. Rev. Lett. 126, 100603 (2021), arxiv:2009.03791 [cond-mat,

- physics:quant-ph].
- [19] L. Masanes, Discrete holography in dual-unitary circuits (2023), arxiv:2301.02825 [cond-mat, physics:gr-qc, physics:hep-th, physics:quant-ph].
- [20] J. Cardy, Nucl. Phys. B **270**, 186 (1986).
- [21] J. L. Cardy, Nuclear Physics B 275, 200 (1986).
- [22] J. L. Cardy, J. Phys. A: Math. Gen. 17, L385 (1984).
- [23] I. Affleck, Phys. Rev. Lett. 56, 746 (1986).
- [24] K. Narayan, Phys. Rev. D 91, 126011 (2015), arxiv:1501.03019 [gr-qc, physics:hep-th].
- [25] K. Narayan, Physics Letters B 753, 308 (2016), arxiv:1504.07430 [hep-th].
- [26] Y. Nakata, T. Takayanagi, Y. Taki, K. Tamaoka, and Z. Wei, Phys. Rev. D 103, 026005 (2021), arxiv:2005.13801 [cond-mat, physics:hep-th, physics:quant-ph].
- [27] K. Doi, J. Harper, A. Mollabashi, T. Takayanagi, and Y. Taki, Timelike entanglement entropy (2023), arxiv:2302.11695 [cond-mat, physics:hep-th, physics:quant-ph].
- [28] K. Doi, J. Harper, A. Mollabashi, T. Takayanagi, and Y. Taki, Phys. Rev. Lett. 130, 031601 (2023), arxiv:2210.09457 [cond-mat, physics:hep-th, physics:quant-ph].
- [29] K. Narayan and H. K. Saini, Notes on time entanglement and pseudo-entropy (2023), arxiv:2303.01307 [hep-th].
- [30] Z. Li, Z.-Q. Xiao, and R.-Q. Yang, J. High Energ. Phys. 2023 (4), 4, arxiv:2211.14883 [gr-qc, physics:hep-th].
- [31] M. C. Bañuls, M. B. Hastings, F. Verstraete, and J. I. Cirac, Phys. Rev. Lett. 102, 240603 (2009).
- [32] A. Müller-Hermes, J. I. Cirac, and M. C. Bañuls, New J. Phys. 14, 075003 (2012), arxiv:1204.5080 [cond-mat, physics:quant-ph].
- [33] M. B. Hastings and R. Mahajan, Phys. Rev. A 91, 032306 (2015), arxiv:1411.7950 [cond-mat, physics:hepth, physics:quant-ph].
- [34] A. Lerose, M. Sonner, and D. A. Abanin, Phys. Rev. X 11, 021040 (2021).
- [35] A. Lerose, M. Sonner, and D. A. Abanin, Phys. Rev. B 107, L060305 (2023).
- [36] S. Carignano, C. R. Marimón, and L. Tagliacozzo, On temporal entropy and the complexity of computing the expectation value of local operators after a quench (2023), arxiv:2307.11649 [cond-mat, physics:quant-ph].
- [37] B. Yan, L. Cincio, and W. H. Zurek, Phys. Rev. Lett. 124, 160603 (2020), arxiv:1903.02651 [quant-ph].
- [38] A. Goussev, R. A. Jalabert, H. M. Pastawski, and D. Wisniacki, Scholarpedia 7, 11687 (2012), arxiv:1206.6348 [cond-mat, physics:quant-ph].
- [39] I. P. McCulloch, J. Stat. Mech. 2007, P10014 (2007).
- [40] B. Pirvu, V. Murg, J. I. Cirac, and F. Verstraete, New J. Phys. 12, 025012 (2010).
- [41] N. F. Robertson, J. Surace, and L. Tagliacozzo, Phys. Rev. B 105, 195103 (2022), arxiv:2110.07078 [cond-mat, physics:hep-th, physics:quant-ph].
- [42] W.-z. Guo, S. He, and Y.-X. Zhang, Relation between timelike and spacelike entanglement entropy (2024), arxiv:2402.00268 [cond-mat, physics:hep-th, physics:quant-ph].
- [43] A. A. Belavin, A. M. Polyakov, and A. B. Zamolodchikov, Nuclear Physics B 241, 333 (1984).
- [44] J. Cardy, Lectures Cardy Les Houches 88 (1988).
- [45] P. Ginsparg, arXiv:hep-th/9108028 (1988), arxiv:hep-th/9108028.

- [46] P. Francesco, P. Mathieu, and D. Sénéchal, Conformal Field Theory, Graduate Texts in Contemporary Physics (Springer-Verlag, New York, 1997).
- [47] M. Henkel, Conformal Invariance and Critical Phenomena, Theoretical and Mathematical Physics (Springer-Verlag, Berlin Heidelberg, 1999).
- [48] J. Cardy, 0807.3472 (2008), arxiv:0807.3472.
- [49] I. Affleck, M. Oshikawa, and H. Saleur, J. Phys. A: Math. Gen. 31, 5827 (1998).
- [50] M. Srednicki, Phys. Rev. Lett. 71, 666 (1993).
- [51] C. Callan and F. Wilczek, arXiv:hep-th/9401072
 10.1016/0370-2693(94)91007-3 (1994), arxiv:hep-th/9401072.
- [52] G. Vidal, J. I. Latorre, E. Rico, and A. Kitaev, Phys. Rev. Lett. 90, 227902 (2003).
- [53] P. Calabrese and J. Cardy, J. Stat. Mech. 2004, P06002 (2004).
- [54] M. Caraglio and F. Gliozzi, J. High Energy Phys. 2008 (11), 076, arxiv:0808.4094 [cond-mat, physics:hep-lat, physics:hep-th].
- [55] M. Grundner, P. Westhoff, F. B. Kugler, O. Parcollet, and U. Schollwöck, Complex Time Evolution in Tensor Networks (2023), arxiv:2312.11705 [cond-mat, physics:quant-ph].
- [56] X. Cao, Y. Lu, E. M. Stoudenmire, and O. Parcollet, Dynamical correlation functions from complex time evolution (2024), arxiv:2311.10909 [cond-mat].
- [57] E. Tirrito, N. J. Robinson, M. Lewenstein, S.-J. Ran, and L. Tagliacozzo, Characterizing the quantum field theory vacuum using temporal Matrix Product states (2022), arxiv:1810.08050 [cond-mat].

- [58] W. Tang, L. Chen, W. Li, X. C. Xie, H.-H. Tu, and L. Wang, Physical Review B 96, 115136 (2017), arxiv:1708.04022 [cond-mat, physics:hep-th].
- [59] A. A. Eberharter, L. Vanderstraeten, F. Verstraete, and A. M. Läuchli, Phys. Rev. Lett. 131, 226502 (2023).
- [60] K. Shinmyo, T. Takayanagi, and K. Tasuki, Pseudo entropy under joining local quenches (2023), arxiv:2310.12542 [cond-mat, physics:hep-th, physics:quant-ph].
- [61] W.-z. Guo, S. He, and Y.-X. Zhang, J. High Energ. Phys. 2022 (9), 94, arxiv:2206.11818 [hep-th].
- [62] J. Surace, M. Piani, and L. Tagliacozzo, Phys. Rev. B 99, 235115 (2019).
- [63] A. Strathearn, P. Kirton, D. Kilda, J. Keeling, and B. W. Lovett, Nat Commun 9, 3322 (2018).
- [64] C. D. White, M. Zaletel, R. S. K. Mong, and G. Refael, Phys. Rev. B 97, 035127 (2018), arxiv:1707.01506 [cond-mat].
- [65] T. Rakovszky, C. W. von Keyserlingk, and F. Pollmann, Dissipation-assisted operator evolution method for capturing hydrodynamic transport (2020), arxiv:2004.05177 [cond-mat].
- [66] M. Frías-Pérez and M. C. Bañuls, Phys. Rev. B 106, 115117 (2022), arxiv:2201.08402 [quant-ph].
- [67] W.-Y. Liu, S.-J. Du, R. Peng, J. Gray, and G. K.-L. Chan, Tensor Network Computations That Capture Strict Variationality, Volume Law Behavior, and the Efficient Representation of Neural Network States (2024), arxiv:2405.03797 [cond-mat, physics:physics, physics:quant-ph].

Supplementary material for

Loschmidt echo, emerging dual unitarity and scaling of generalized temporal entropies after quenches to the critical point

Stefano Carignano
Barcelona Supercomputing Center, 08034 Barcelona, Spain*

 ${\rm Luca~Tagliacozzo} \\ {\it Institute~of~Fundamental~Physics~IFF-CSIC,~Calle~Serrano~113b,~Madrid~28006,~Spain}^{\dagger}$

CFT PREDICTIONS FOR A CYLINDER

For completeness, we recall here CFT predictions for an infinite temperature boundary state, which would result in an infinite cylinder geometry. From the TN point of view, we can represent it using the same algorithm employed in this manuscript by folding the cylinder, similar to what proposed in [1]. The infinite cylinder described by complex coordinate w=s+iu is related to the 2D plane by the conformal map $w=\frac{v\beta}{2\pi}\log(z)$, and the transfer operator in this case is given by

$$\mathcal{T} = \exp\left[-\frac{\kappa}{\beta v} + \frac{2\pi}{\beta v}(L_0 + \bar{L}_0)\right],\tag{1}$$

where $\kappa = -\pi c \delta t/6$. We will present the corresponding numerical results elsewhere.

TN SETUP, SYMMETRIC MPO

In this section we briefly describe the methods used in this work for building the MPO of the transition matrix \mathcal{T} and extract its eigenvalues. The concrete algorithm was introduced in [2] inspired on those presented in [1, 3]. It is basically a power method that iteratively applies the transfer matrix \mathcal{T} to an initial MPS state and uses a low rank approximation of the reduced transition matrices in order to compress the MPS.

Our temporal MPO \mathcal{T} is defined by contracting one column of the infinite tensor network shown in Fig. 2 in the main text, containing $N_T + 2N_\beta$ (with $N_\beta = \beta_0/\delta t$) tensors. The basic ingredients for the MPO are the tensors $W_i(\delta t)$ associated with a given site and timestep, building up the time evolution operator $U(\delta t)$ (see Fig. 1 in the main text).

Since we work with translationally invariant systems, there is no explicit space dependence, and all tensors have the same dependence on δt . The only inhomogeneities in the time direction are induced by the initial state $|\psi_0\rangle$, which we take as a product state.

For a gapped \mathcal{T} , the intensive Loschmidt echo converges exponentially fast to $l = -|\lambda_0|/T$ and in order to extract λ_0 we use an MPS ansatz for the dominant eigenvectors $|R\rangle$ and $\langle L|$ of \mathcal{T} .

The roles of virtual and physical legs are interchanged if one performs a transverse contraction, as the temporal MPO \mathcal{T} is applied sideways to the boundary MPS which will result in the dominant left and right vectors. In this sense, an asymmetry in the virtual legs of the MPO tensors will result in a left dominant vector for \mathcal{T} which is different from the right one, ie. $|L\rangle \neq |R\rangle$. Nevertheless, we were able to work with tensors which are symmetric on both the physical and virtual legs, so that this additional complication does not arise. More specifically, for the Ising model we employ the compact representation proposed in [5] at second-order in the Trotter expansion, for which we obtain for the MPO tensors

$$W = \begin{pmatrix} \cos(\delta t)(a\mathbf{1} + b\sigma_z) & \sqrt{i\sin(\delta t)\cos(\delta t)}\sigma_x \\ \sqrt{i\sin(\delta t)\cos(\delta t)}\sigma_x & i\sin(\delta t)(a\mathbf{1} + b\sigma_z) \end{pmatrix}, (2)$$

with $a = 1 - 2\sin(g\delta t/2)^2$, $b = 2i\sin(g\delta t/2)\cos(g\delta t/2)$.

The generalization of this type of construction unfortunately would not lead to a symmetric left-right MPO in the case of the Potts model, due to the presence of both σ_i and σ_i^{\dagger} terms (cfr. Eq. (11) in the main text). Nevertheless, we are still able to extract a symmetric expression by considering the two-body operator $U_{i,i+1}(\delta t)$ and separating it via a symmetric SVD factorization. The resulting MPO tensors are again symmetric in both physical and virtual legs.

Being able to work in this symmetric gauge in which $\bar{\mathcal{T}} = \mathcal{T}^t$ (where the bar denotes complex conjugation), we can thus focus on extracting $|R\rangle$ and then obtain $\langle L| = \langle \bar{R}|$ by a simple transposition. This also significantly improves the numerical stability of our TN simulations (see eg. [4] and references therein for a discussion on the challenges presented by non-hermitian eigenvalue problems).

Having obtained the form of the transfer matrix tensors, we build the transverse MPO for \mathcal{T} by incorporating N_{β} steps of imaginary time $(\delta t \to -i\delta\beta_0)$ at the edges of the TM, where the real time evolution is performed in the center.

The determination of the dominant eigenvalues of \mathcal{T} was performed via a symmetric power method algorithm which simply goes as follows: starting from an initial guess for the right dominant vector $|R\rangle$ in the form of MPS along the temporal direction, at each iteration \mathcal{T} is

applied to $|R\rangle$ and the resulting MPS is truncated by optimizing the overlap $\langle \bar{R}|R\rangle$, since, as already discussed, in our case we have $\langle L|=\langle \bar{R}|.$ This is done by appropriately truncating on the singular values of the reduced transition matrices, Eq.(8) main text (see [2] for additional details). The iterations are repeated until convergence is reached, and the eigenvalues of the transition matrices are used to compute the entropies along the temporal chains.

FITS ON REAL PARTS OF THE DOMINANT EIGENVALUES.

By fitting the real part of the dominant eigenvalues of \mathcal{T} we can get further confirmation of our CFT predictions, although the procedure is a bit more involved. When it comes to the real parts, by comparing with Eq. (4) in the main text we see that a single term $a_0 = 2\beta_0 av + b$ does not allow us to resolve the pieces involved, but we can extract some additional information by looking at the difference of the real parts for different values of β_0 . Indeed, if we consider $\Delta_\beta \lambda_0 \equiv \lambda_0^{\beta_0 \equiv \beta_1} - \lambda_0^{\beta_0 \equiv \beta_2}$, we expect that $Re(\Delta_\beta \lambda_0) = 2a(\beta_1 - \beta_2) + \mathcal{O}(1/T^2)$, whereas $Im(\Delta_\beta \lambda_0) = \mathcal{O}(1/T^3)$.

We thus fit the difference of the real part for different values of β with a functional form $f_2 = b_0 + b_2/T^2$. As an example, we fit for the Ising model, for the case $\Delta_{\beta}\lambda_0(\beta=0.4-\beta=0.2)$ we get $b_0=0.51$, whereas for $\Delta(\beta=0.6-\beta=0.2)$ we find $b_0=1.02$, showing again an excellent agreement with the CFT prediction which indeed gives a ratio of 2 between the two values.

At this point, we can also extract the non-universal coefficient $a = b_0/2(\beta_1 - \beta_2) \simeq 1.275$ from here, which is consistent with the a_0 from the fit of the imaginary part above.

CORRECTIONS TO THE LEADING FINITE SIZE SCALING FOR THE GENERALIZED ENTROPIES

The rate at which our results approach the CFT predictions of the generalized entropies is affected by the choice of initial state for the Loschmidt echo , which can be associated with different boundary CFT states and as a result with a different operator content of the theory. As an example, we show in Fig. S1 the curves obtained for Ising and Potts using fixed BC. There we can appreciate that the convergence to the CFT results is significantly slower than the corresponding one for free BC, particularly for approach of the imaginary part to the expected constant value.

Such large deviations are quite usual in the context of studying the scaling of the entanglement entropy in different scenarios [6-10]. Here we show that even for

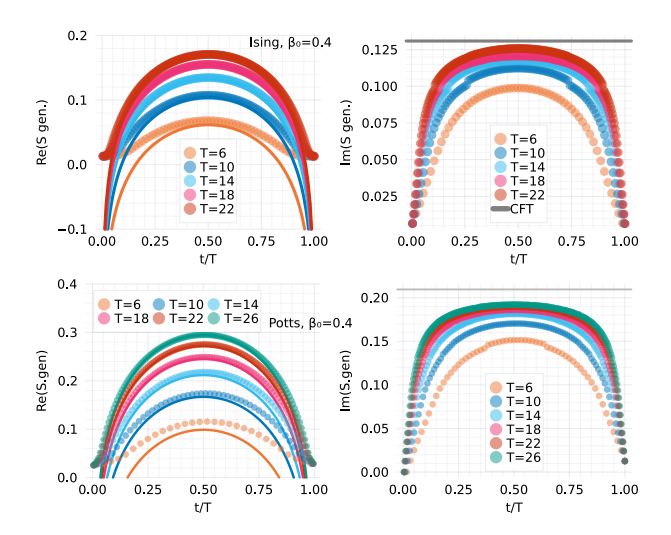


FIG. S1. Numerical results for the real (left) and imaginary (right) parts of the generalized entropies for the critical Ising (top row) and Potts (bottom row) with fixed BC. Thick solid lines denote the CFT predictions.

generalized entropies such corrections are induced by finite size effects and vanish as inverse powers of the IR and UV cutoff. We expect indeed that both a finite β_0 and T to introduce perturbations to our system. In the following, we will focus on the distance between the numerical results from our TN simulations for the imaginary part (taken at midchain) and the expected CFT result, ie. $\Delta S = Im(S_{gen})_{CFT} - Im(S_{gen})_{TN}$ even if one could work with the full chain length, in order to study the approach of all the points to the CFT results.

In order to investigate the effect of T, we can use the standard analysis described in [6]: In particular, we expect that the leading corrections should scale as some inverse power of $\Delta S \propto T^{-x}$, with x the lowest neutral relevant field. This implies that for Ising $x=1=\Delta_{\epsilon}$, while for Potts we expect $x=4/5=\Delta_{\epsilon}$.

Our numerical results for Ising, as well as for Potts with fixed BC are indeed consistent with this kind of prediction, see Fig. S2.

Now we can add the effects of finite β_0 : since β_0 plays the role of a UV cut-off, we now expect corrections $\Delta S \propto \beta_0^{\gamma}$ with γ the scaling dimension of the most relevant operator coupling to ΔS . Putting everything together we thus expect that the scaling variable for the correction should be $\beta_0^{\gamma/x}/T$.

Performing our fits, we find that for Ising with free BC an exponent $\gamma=1.5$ which is compatible with $\gamma=2-\Delta'_{\sigma}$, where $\Delta'_{\sigma}=0.5$ is the boundary magnetization. For fixed BC on the other hand our best fit suggests $\gamma=0.5$. For Potts with fixed BC initial state we find instead $\gamma=2/5$, which once more is compatible with Δ_{ϵ} . The exponents change as expected for the Potts model with free BC: there the best fits give an exponent $x \simeq 4/3$ (compatible

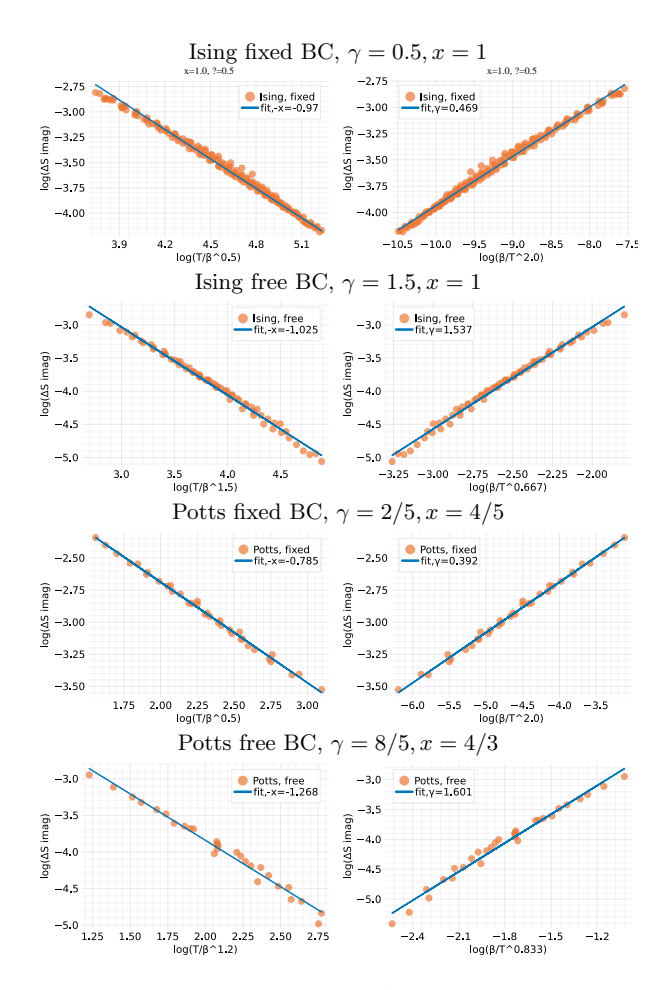


FIG. S2. Scaling behavior for ΔS , the difference of the imaginary part (at mid-chain) of the Ising (first rows) and Potts (bottom rows) entropies with the respect to the CFT predictions, for fixed and free boundary conditions. ΔS for the various cases are plotted as function of $T/\beta_0^{\gamma/x}$ (left) and of $\beta_0/T^{x/\gamma}$ (right). The coefficients resulting from the best fits are shown in the plots.

with a neutral para-fermion condensate) and $\gamma \simeq 8/5$, which is compatible with $\gamma = 2 - 2/5$, see Fig. S2

- * stefano.carignano@bsc.es
- † luca.tagliacozzo@iff.csic.es
- M. C. Bañuls, M. B. Hastings, F. Verstraete, and J. I. Cirac, Phys. Rev. Lett. 102, 240603 (2009).
- [2] S. Carignano, C. R. Marimón, and L. Tagliacozzo, On temporal entropy and the complexity of computing the expectation value of local operators after a quench (2023), arxiv:2307.11649 [cond-mat, physics:quant-ph].
- [3] M. B. Hastings and R. Mahajan, Phys. Rev. A 91, 032306 (2015), arxiv:1411.7950 [cond-mat, physics:hepth, physics:quant-ph].
- [4] W. Tang, F. Verstraete, and J. Haegeman, Matrix Product State Fixed Points of Non-Hermitian Transfer Matrices (2023), arxiv:2311.18733 [cond-mat, physics:quantph].
- [5] B. Pirvu, V. Murg, J. I. Cirac, and F. Verstraete, New J. Phys. 12, 025012 (2010).
- [6] J. Cardy and P. Calabrese, Journal of Statistical Mechanics: Theory and Experiment 2010, P04023 (2010).
- [7] V. Alba, L. Tagliacozzo, and P. Calabrese, Physical Review B 81, 60411 (2010).
- [8] V. Alba, L. Tagliacozzo, and P. Calabrese, Journal of Statistical Mechanics: Theory and Experiment 06, 012 (2011).
- [9] P. Calabrese, L. Tagliacozzo, and E. Tonni, J. Stat. Mech. 2013, P05002 (2013).
- [10] A. Coser, L. Tagliacozzo, and E. Tonni, J. Stat. Mech. 2014, P01008 (2014).